phys. stat. sol. (b) **122**, 317 (1984)

Subject classification: 10.2 and 19; 22.8.1

Twente University of Technology,
Laboratory of Inorganic Chemistry and Materials Science, Enschede[1])

The Simulation and Interpretation of the EPR Powder Spectra of Gd^{3+}-Doped $LaAlO_3$

By

H. J. A. KOOPMANS, M. M. A. PERIK, B. NIEUWENHUIJSE, and P. J. GELLINGS

The EPR powder spectra of Gd^{3+} doped $LaAlO_3$ are simulated for a number of temperatures between 4 and 800 K by means of the usual spin-Hamiltonian. Values are found for the zero field splitting parameters $B(n, 0)$ only, which agree with single crystal measurements. For an accurate simulation of the axial powder spectra a variable linewidth has to be introduced, because an inhomogeneous broadening of the resonances in the xy plane is observed. This broadening is successfully described by a variable $B(2, 2)$ parameter. This indicates that the Gd^{3+} ion does not fit within the $LaAlO_3$ lattice, because $GdAlO_3$ is not isostructural with $LaAlO_3$. Crystal field calculations support this assumption.

Die EPR-Pulver-Spektren, der mit Gd^{3+} dotierten Verbindung $LaAlO_3$, werden für einige Temperaturen zwischen 4 und 800 K mit dem üblichen Spin-Hamiltonoperator simuliert. Nur für die Nullfeldaufspaltung der Parameter $B(n, 0)$ werden Werte gefunden, die mit Messungen an Einkristallen übereinstimmen. Um eine gute Simulation der axialen Spektren des Polykristalls zu erhalten, ist eine variable Linienbreite nötig, weil eine inhomogene Verbreiterung in der (x, y)-Ebene beobachtet wird. Diese Verbreiterung wird erfolgreich durch verschiedene $B(2, 2)$ Parameter beschrieben. Daraus läßt sich schließen, daß das Gd^{3+}-Ion sich nicht in das $LaAlO_3$-Gitter einfügt, da die Gitterstrukturen von $GdAlO_3$ und $LaAlO_3$ nicht übereinstimmen. Berechnungen des Kristallfeldes unterstützen diese Behauptung.

1. Introduction

Although considerable research has been done in the field of the interpretation of EPR spectra of transition metal ions doped in a large variety of compounds, only in rare cases this has been done on powders. Nevertheless, in practice powders are more widely used than single crystals and therefore deserve more attention. At this laboratory ceramics are investigated with interesting ferroelectric, piezo-electric, or ionic conducting properties for use in electronic devices [1 to 3]. These properties are strongly related with the usually complex composition and structure. To investigate the local atomic structure of these compounds an EPR study has been started of paramagnetic ions doped in these materials. In earlier reports [4, 5] the EPR spectrum of polycrystalline $PbTiO_3$ doped with Gd^{3+} ions has been described successfully in terms of zero field splitting parameters. Unfortunately, the observed parameters for this compound, when compared with those calculated from the crystal field theory, could be explained both by introducing distortions in the crystal lattice and by the presence of Pb^{2+} vacancies needed for charge compensation.

To exclude the second possibility $LaAlO_3$ has been chosen as a new model compound with the purpose to gather more experience in simulating and interpreting EPR powder spectra. $LaAlO_3$ is rarely used in electronic devices (an example is as capacitor

[1]) P.O.B. 217, 7500 AE Enschede, The Netherlands.

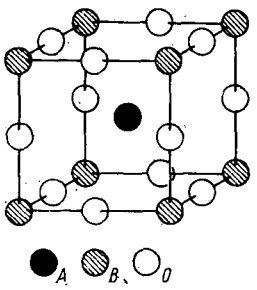

Fig. 1. Ideal perovskite structure ABO_3

material [6]), but this compound is very interesting due to its second-order structural phase transition [7]. The structure of $LaAlO_3$, which belongs to the large family of perovskites ABO_3 (Fig. 1), has been described by several authors [8 to 11]. Above the phase transition temperature $T_c = 795$ K [12] the structure is cubic (ideal perovskite), while beneath T_c a rhombohedral deformation appears and according to Derighetti et al. [10] the space group is $R\bar{3}c$ then.

The continuous change of the deformation makes $LaAlO_3$ particularly suited for studying its properties by EPR powder spectra. Gd^{3+} has been chosen as the paramagnetic tracer ion due to its well-defined charge and its applicability over a large temperature range [7]. Low and Zusman [13] have already published some results from measurements on single crystals doped with this ion. This offers a possibility to check the spin-Hamiltonian parameters. Besides, these parameters have also been verified by simulations of the powder spectra.

The phase transitions, which are frequently observed in perovskites, are usually described in terms of rotations of the BO_6 octahedra about one or more symmetry axes [7, 14]. For example, the phase transition in $LaAlO_3$ is described as a rotation of the AlO_6 octahedra around a C_3-symmetry axis in accord with the symmetry of the space group. Although the interaction of the Gd^{3+} ions with their environment is not quite well understood [15], it is tried to find a relation between the observed spin-Hamiltonian parameters and the structure of $LaAlO_3$ by crystal field potential calculations and the superposition model of Newman [15]. For this purpose some structural parameters have been acquired by X-ray and neutron diffraction techniques.

2. Experimental

$La_{1-x}Gd_xAlO_3$ compounds with $x = 0$, 0.0025, 0.005, and 0.01 have been synthesized by a solid state reaction of the pure oxides for 100 h at 1550 °C [16]. Guinier photographs showed the perovskite structure of $LaAlO_3$ without traces of other compounds or unreacted oxides. X-ray fluorescence analysis showed close agreement with the desired composition. The sample with $x = 0.0025$ gave the best results for the EPR spectra with respect to linewidth and intensity. Therefore, only this sample has been examined in detail. Composition analysis of this sample: La 64.28% (64.77%), Al 12.69% (12.61%) and Gd 0.25% (0.18%) (theoretical values within parentheses).

The EPR experiments at X-band from 4 K up to room temperature have been performed with a Varian E-12 spectrometer and an Oxford Instruments cooling unit [17]. At higher temperatures a Varian E-15 spectrometer has been employed with a high-temperature cavity developed by Koningsberger et al. [18]. Q-band spectra have been recorded with a Varian E-12 spectrometer at room temperature only. Microwave frequencies have been measured with Hewlett Packard frequency counters. All samples have been examined in normal quartz tubes. The magnetic field has been measured

with an "AEG-Kernresonanz-Magnetfeldmesser" and the temperature with a Cu–constantan thermocouple except at liquid helium temperature. In that case an Au(0.03 at % Fe)–chromel couple has been used [19]. Because the sensitivity of this couple changes in electric and magnetic fields, the temperature of the sample could not be measured in situ but only the temperature of the He gas flow. Therefore, the real temperature of the sample might have been somewhat higher because of heat leaks.

X-ray photographs have been taken with a Guinier-Simon camera using Cu–$K_{\alpha 1}$ radiation and a 4 mm diaphragm. The determination of the lattice constant has been made from the measurement of the high angle lines ($2\theta = 35°$ to $110°$) with α-Al_2O_3 as a reference. The sample tube consisted of a capillary of 0.2 mm diameter.

A neutron scattering experiment has been performed at $T = 300$ K with the powder diffractometer at the Petten high flux reactor, using neutrons of wavelength $\lambda = 2.5903(3)$ Å and a $LaAlO_3$ sample without Gd^{3+}. Experimental details have been described elsewhere [20]. Data have been collected in the range $5° < 2\theta < 155°$ in steps of 0.1°. The diffraction patterns were analysed by means of the Rietveld method [21] using neutron scattering lengths published by Bacon [22].

The parameters in the refinement were a scale factor c, three half-width parameters defining the Gaussian lineshape, the counter zero error, the unit cell parameters, the atomic positional parameter, and isotropic temperature factors. By minimizing the function $x^2 = \sum \omega[y(\text{obs}) - (1/c)\, y(\text{calc})]^2$, this yielded the following R-factor:

$$R_{\text{profile}} = \frac{\sum \left| y(\text{obs}) - \left(\frac{1}{c}\right) y(\text{calc}) \right|}{\sum y(\text{obs})} = 4.37\% ,$$

where y(obs) and y(calc) are the observed and calculated profile data points and ω is the statistical weight alloted to each data point.

All calculations have been performed on a DEC-10 computer with a central core of 256 k words of 35 bits.

3. Theoretical Considerations

The EPR powder spectrum of the Gd^{3+} ion, which has the ground state $^8S_{7/2}$, can be described with the spin-Hamiltonian [23]

$$\mathcal{H} = \beta \boldsymbol{H} \boldsymbol{g} \hat{\boldsymbol{S}} + \sum_{n=2,4,6} \sum_{m=-n}^{+n} B(n, m)\, \hat{O}(n, m) \tag{1}$$

in which $\hat{\boldsymbol{S}}$ is the spin operator and $\hat{O}(n, m)$ are the Stevens equivalent operators [24]. The $B(n, m)$ parameters are the zero field splitting parameters, which have to be determined. Terms for the hyperfine splitting, nuclear Zeeman interaction, etc. have been omitted, because the splitting due to these terms is much smaller than the linewidth observed in the powder spectra (at least 3 mT).

For the evaluation of the spectral parameters a general purpose computer program called EPRALL has been used [5]. This program calculates the magnetic field values of the resonances and the corresponding transition probabilities, when a set of parameters is introduced. By means of a parameter stepping procedure the best set of parameters can be obtained. This is achieved by minimizing a root-mean-square parameter R given by (2) and found from the differences between calculated (H_c) and

observed (H_0) resonance fields,

$$R = \left[\frac{\sum_i f_i \left[\frac{H_{0i} - H_{ci}}{\Delta H_{0i}} \right]^2}{(\sum_i f_i) - p} \right]^{1/2} . \tag{2}$$

In this equation ΔH_0 is the uncertainty of H_0, f indicates whether or not a calculated line is observed, and p is the number of non-zero parameters. The program also generates angular data in order to calculate the extra lines, belonging to orientations of the magnetic field other than the principal axes. By means of a separate program VARWID these data can be added for an axial case, in order to find the absorption intensity I as a function of the magnetic field. An axial spectrum is defined as a spectrum, for which the resonance field values are independent of the angle φ, if a crystal is rotated in a magnetic field. The angle φ is one of polar angles (θ, φ) describing the direction of the magnetic field relative to a coordinate system in the crystal. The intensity I is now proportional to the probability to find a resonance between the values H and $H + \mathrm{d}H$ [25],

$$I \sim \sin\theta \frac{\mathrm{d}\theta}{\mathrm{d}H} T(\theta) , \tag{3}$$

where θ is the angle between the direction of the magnetic field and the main symmetry axis in the crystal (usually assigned as the z-axis), for which this resonance value H is found, and $T(\theta)$ the transition probability of this resonance. After introduction of a Lorentzian linewidth, a simulation of the derivative powder spectrum can be obtained.

Before any X-band spectrum of Gd^{3+}-doped $LaAlO_3$ was examined, first a rough interpretation was given of the Q-band spectrum at room temperature. Due to the larger splitting of the Zeeman term in the latter case, a clearer separation of the allowed transitions from "forbidden" transitions is obtained. After Reynolds et al. [26] the splitting of the resonances can be described for orthothombic symmetry at a first approximation for $\boldsymbol{H} \parallel \boldsymbol{z}$ by the equations

$$\begin{aligned}
\left| \Delta H \left(\frac{7}{2}, \frac{5}{2} \right) \right| &= \frac{12b(2,0) + 40b(4,0) + 12b(6,0)}{g_{\parallel}\beta} , \\
\left| \Delta H \left(\frac{5}{2}, \frac{3}{2} \right) \right| &= \frac{8b(2,0) - 20b(4,0) - 28b(6,0)}{g_{\parallel}\beta} , \\
\left| \Delta H \left(\frac{3}{2}, \frac{1}{2} \right) \right| &= \frac{4b(2,0) - 24b(4,0) + 28b(6,0)}{g_{\parallel}\beta} ,
\end{aligned} \tag{4a}$$

and for $\boldsymbol{H} \perp \boldsymbol{z}$ by

$$\begin{aligned}
\left| \Delta H \left(\frac{7}{2}, \frac{5}{2} \right) \right| &= \frac{6b(2,0) - 15b(4,0) + \frac{15}{4} b(6,0) - 6b(2,2)\cos 2\varphi}{g_{\perp}\beta} , \\
\left| \Delta H \left(\frac{5}{2}, \frac{3}{2} \right) \right| &= \frac{4b(2,0) + \frac{15}{2}(4,0) - \frac{35}{4} b(6,0) - 4b(2,2)\cos 2\varphi}{g_{\perp}\beta} , \\
\left| \Delta H \left(\frac{3}{2}, \frac{1}{2} \right) \right| &= \frac{2b(2,0) + 9b(4,0) - \frac{35}{4} b(6,0) - 2b(2,2)\cos 2\varphi}{g_{\perp}\beta} ,
\end{aligned} \tag{4b}$$

where $|\Delta H(M_s, M_s - 1)| = |H(M_s \rightarrow M_s - 1) - H(-M_s + 1 \rightarrow -M_s)|$ and the $b(n, m)$ are defined by

$$b(2, m) = 3B(2, m) ,$$

$$b(4, m) = 60B(4, m) ,$$

and

$$b(6, m) = 1260B(6, m) .$$

The resulting set of approximate parameters has been used as a starting set for the least squares refinement by (2).

4. Results

The powder spectra of Gd^{3+}-doped $LaAlO_3$ have been measured at several temperatures between 4 and 900 K. By means of (4) the observed resonances in the Q-band spectrum have been assigned (Fig. 2). The $b(2, 0)$ parameter has arbitrarily been taken as positive and the signs of the other parameters are relative to this parameter. The resulting set of approximate parameters has been used to index the resonances in the corresponding X-band spectrum. The gradual change of the powder spectrum, due to the second-order phase transition facilitated the interpretation at other temperatures. Within the experimental accuracy values have been found for the $b(n, 0)$ parameters only for all temperatures by applying (2). For example the calculated and observed resonance field values are shown in Table 1 for the EPR powder spectrum at 4 K, where the splitting of the resonances is largest. The calculated differences

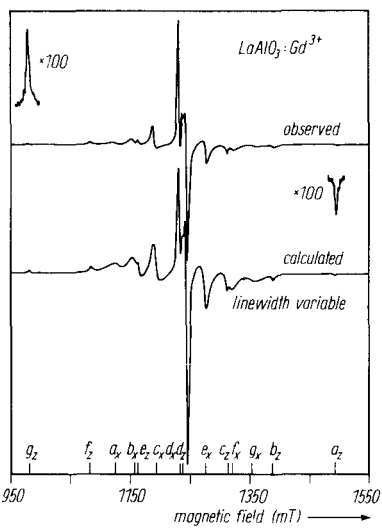

Fig. 2

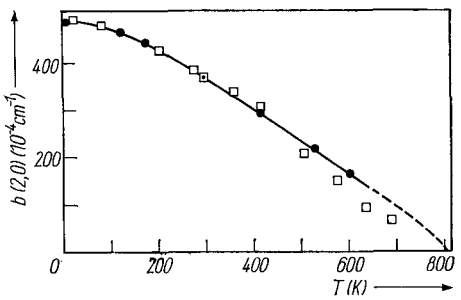

Fig. 3

Fig. 2. Observed and calculated EPR powder spectra of Gd^{3+}-doped $LaAlO_3$ at Q-band. The positions of the calculated resonances for $M_s \rightarrow M_s - 1$ transitions are also indicated for specific orientations of the magnetic field (x or z). The transitions are designated by a letter according to the following code: a: $M_s = -5/2 \rightarrow -7/2$, b: $-3/2 \rightarrow -5/2$, c: $-1/2 \rightarrow -3/2$ d: $1/2 \rightarrow -1/2$, e: $3/2 \rightarrow 1/2$, f: $5/2 \rightarrow 3/2$, g: $7/2 \rightarrow 5/2$. Frequency 34.464 GHz, $T = 293$ K

Fig. 3. The zero field splitting parameter b (2,0) as a function of temperature for $LaAlO_3$:Gd^{3+}. ● this work, □ Low and Zusman [13]

Table 1

Observed (H_0) and calculated resonances (H_c) of the EPR powder spectrum of Gd^{+3}-doped $LaAlO_3$ at 4 K. The transitions (tr) are indicated as in Fig. 2. The R-value of the fit as defined by (4) comes to 2.47 for the resonances indicated with $f = 1$

tr	θ	H_0 (mT)	H_c (mT)	ΔH (mT)	f	tr	θ	H_0 (mT)	H_c (mT)	ΔH (mT)	f
f	0°	123.0	124.4	−1.4	1	d	39°	373.0	375.9	−2.9	0
a	90°	204.0	203.5	0.5	1	f	90°	412.4	414.7	−2.3	1
e	0°	—	225.1	—	0	f	85°	412.4	415.1	−2.7	0
b	90°	229.2	227.9	1.3	1	c	0°	424.7	423.7	1.0	1
c	90°	257.4	256.7	0.7	1	c	18°	431.5	431.7	−0.2	0
d	90°	296.2	294.7	1.5	1	g	90°	492.0	494.4	−2.6	1
d	0°	324.4	324.4	0.0	1	b	0°	524.9	524.4	0.5	1
e	90°	349.0	348.1	0.9	1	b	4°	524.9	524.5	0.4	0
e	63°	373.0	368.2	4.8	0	a	0°	654.3	653.0	1.3	1

are well within the observed linewidth of at least 3 mT. The final results of the refinements for all measured temperatures is given in Table 2.

Inspection of Table 2 shows that the isotropic g-values agree very well with the theoretical value 1.993 ± 0.002 [15], whereas only the $b(2, 0)$ parameter is significantly temperature dependent. The observed $b(2, 0)$ values are in excellent agreement with the single crystal measurements of Low and Zusman [13] at least at lower temperatures (Fig. 3). The discrepancies at higher temperatures are probably due to the fact that these authors could not keep the temperature constant for sufficiently long times to complete the measurement of all transitions. The highest temperature, at which the splitting was resolved sufficiently to derive the spin-Hamiltonian parameters, was about 600 K in this investigation. Above this temperature the splitting was too small with respect to the linewidth. However, careful extrapolation to $b(2, 0) = 0$ ("cubic" surrounding of the Gd^{3+} ion) yields a transition temperature of about 800 K in agreement with the powder diffraction data of Geller and Raccah [12]. Above this temperature no changes have been observed in the ESR powder spectrum which consists of a single sharp line at $g = 1.991$ (1) with a shoulder at each side.

Table 2

Spin-Hamiltonian parameters for Gd^{3+} doped in polycrystalline $LaAlO_3$ at several temperatures. The signs of the $b(n, 0)$ parameters are relative to the unknown sign of $b(2, 0)$

T (K)	freq. (MHz)	g	$b(2, 0)$	$b(4, 0)$ (10^{-4} cm^{-1})*)	$b(6, 0)$
4	9040.7	1.991 (2)**)	486.6 (1.0)**)	6.2 (1.0)**)	1.7 (0.5)**)
118	9117.3	1.990	466.5	5.5	1.5
168	9117.6	1.990	443.4	6.0	1.5
293	9106.0	1.992	370.1	6.2	1.0
413	9164.4	1.991	294.1	5.9	1.1
526	9163.5	1.990	218.2	6.0	1.0
600	9162.8	1.989	164.6	5.8	0.9

*) $b(2, 0) = 3B(2, 0)$, $b(4, 0) = 60B(4, 0)$, and $b(6, 0) = 1260B(6, 0)$.

**) Accuracy the same for all temperatures.

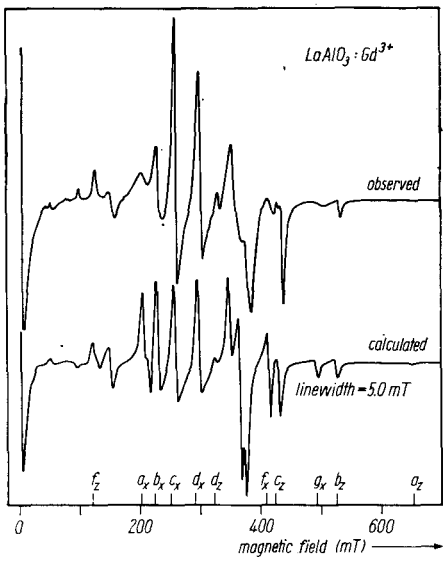

Fig. 4. Observed and calculated EPR powder spectra of Gd^{3+}-doped $LaAlO_3$ at 4 K. The transitions are designated as indicated in Fig. 2. Frequency 9.041 GHz, $T = 4$ K

Because only the $b(n, 0)$ parameters have been found, these parameters can be checked by an axial simulation of the powder spectrum. For $T = 4$ K the observed and calculated powder spectra are shown in Fig. 4. Although the resonance positions are calculated within the experimental accuracy (Table 1), a rather poor simulation is obtained with respect to the intensities. For the transitions, which are assigned to directions perpendicular to the z-axis, a broadening, which is different for different resonances, is observed. To explain the origin of this broadening, some additional experiments have been performed. These show the following facts:

— The broadening is insensitive to differences in the preparation technique. The same broadening has been observed in samples prepared by the solid state reaction of the mixed oxides [16], by the citrate method [27], and even by powdering a "single" crystal. This highly twinned single crystal has been prepared by the zone melting technique [28].

— The broadening is almost insensitive to small or large deviations from stoichiometry. A few samples with general formula $La_{1-x+y}Gd_x\,Al_{1-y}O_3$ have been synthesized with $-0.83 < y < 0.33$ and $x = 0.0025$. For $y > 0$ a combination of the powder spectra of La_2O_3 and $LaAlO_3$ has been observed, whereas for $y < 0$ only the spectrum of $LaAlO_3$ has been obtained in agreement with the phase diagram of the system La_2O_3–Al_2O_3 [29]. Only in the latter case a slight increase of the linewidth has been observed with decreasing y.

— The broadening increases with increasing concentration of the Gd^{3+} ions. This is expected from the increased spin–spin interaction. However, the same broadening has been observed in all transitions irrespective of the direction of the magnetic field relative to the main symmetry axis and therefore this broadening cannot explain the unusual broadening.

— The sample without Gd^{3+} also showed an EPR spectrum which appeared to be due to Fe^{3+} ions present as impurities in the Al_2O_3 used. Samples with deliberately increased amounts of Fe^{3+} ions in $La_{1-x}Gd_xAlO_3$ showed the sum of two spectra due to both the Fe^{3+} and Gd^{3+} ions. There was no indication for any interaction between the different paramagnetic ions.

— An excellent simulation of the powder spectra has been obtained after the introduction of a variable linewidth. Fig. 4 shows that the transitions in the (x, y) plane between states with large M_S values are broadened more than the $M_S = +\frac{1}{2} \rightarrow -\frac{1}{2}$ transition (d_x). Therefore, it is likely that this variable linewidth can be correlated with a $b(2, 2)$ parameter, because only this parameter splits the transitions in that way. However, the introduction of a well defined $b(2, 2)$ parameter and a normal linewidth produces a splitting of the resonances, which is not experimentally observed. There-

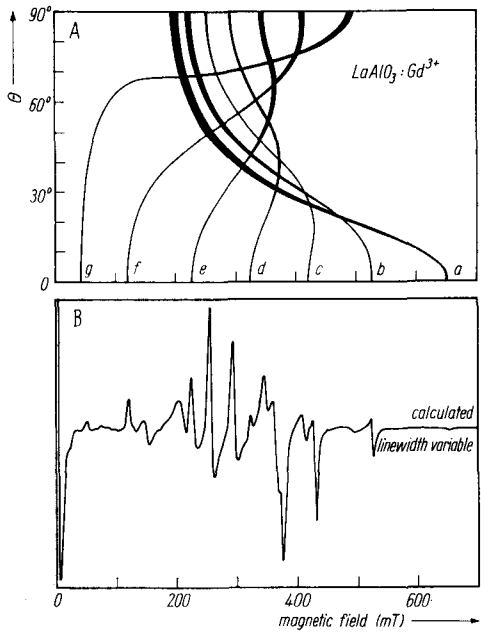

Fig. 5. A) Calculated resonance positions for Gd^{3+}-doped $LaAlO_3$ at 4 K (frequency 9.041 GHz) as a function of θ. The relative dependence of the resonances to the $b(2, 2)$ parameter is indicated by the thickness of the lines. B) Calculated EPR powder spectrum of Gd^{3+}-doped $LaAlO_3$ at 4 K by means of a variable linewidth

fore, it seems that there is no particular value for this parameter, but rather a set of values distributed around the average value zero. This latter statement is imposed by the fact that the resonance field values have been predicted correctly already. Such a distribution of $b(2, 2)$ parameters can be understood if the Gd^{3+} ions are located at a large number of sites, which differ only very slightly from each other.

Fig. 5A shows the splitting of the resonances due to an arbitrary $b(2, 2)$ parameter for the EPR spectrum at 4 K, as a function of the angle θ between the magnetic field vector and the principal axis of symmetry (z-axis). This splitting is depicted as a broadening of the resonances to represent the distribution in the $b(2, 2)$ parameters. So the thickness of the lines indicates the relative dependence of a resonance field value to the $b(2, 2)$ parameter. Because no well-defined $b(2, 2)$ parameter can be derived, the observed EPR powder spectrum has been simulated by means of a variable linewidth to account for the distribution of the parameters. The linewidth ΔH can now be described for each transition $M_s \rightarrow M_s - 1$ at each orientation θ by

$$\Delta H(M_s, \theta) = \Delta H_0 + \Delta H\big(b(2, 2)\big) , \tag{5}$$

where ΔH_0 is the usual linewidth for powders (3 to 4 mT) and $\Delta H\big(b(2, 2)\big)$ is the part of the linewidth which depends on the splitting due to the $b(2, 2)$ parameter. This parameter has been adjusted so that visually a reasonable simulation is obtained. The value of $b(2, 2)$ (used in this sense) decreases with increasing temperature. The same principle has successfully been applied for the Q-band spectrum as indicated in Fig. 2. In all these calculations the intensity I (equation (3)) has been taken inversely proportional to the linewidth, because the total intensity of each resonance has to remain constant irrespective of the attributed linewidth [30].

4.1 Interpretation of the b(n, m) parameters

According to the electrostatic point charge model as described by Hutchings [31], the zero field splitting parameters are related to the crystal field parameters by the equation

$$B(n, m) = A(n, m) \langle r^n \rangle \theta_n , \tag{6}$$

where $\langle r^n \rangle$ can be calculated from the 4f wave functions [32], and θ_n is a factor depending on n, the number and orbital quantum numbers of the electrons of the central ion,

and on the total quantum number J. $A(n, m)$ are the crystal field parameters which depend on the charge q and the position (R, θ, φ) of the surrounding ions and are given by

$$A(n, m) = -|e| \, C_{nm} \frac{4\pi}{2n + 1} \sum_j \frac{q_j}{R_j^{(n+1)}} \, Z(n, m, \theta_j, \varphi_j) \, . \tag{7}$$

C_{nm} are constants depending on n and m, and $Z(n, m)$ are the tesseral harmonics. Unfortunately, the factor θ_n is zero for a pure S ground state. Therefore, the observed splittings are due to second-order effects.

The electrostatic potential of the surrounding ions is only one of these effects [33]. However, the electrostatic point charge model has been used with some success in the explanation of the splittings observed in the system $PbTiO_3:Gd^{3+}$, which shows an axial powder spectrum, too [5]. For that reason the $A(n, m)$ parameters have also been calculated in this case.

Whatever the model used to interpret the observed spin-Hamiltonian parameters a detailed knowledge of the structure is always necessary. Therefore, the lattice constants have been measured at 113 K to extend the high-temperature cell parameters of Geller and Raccah [12]. In Table 3 the lattice constants are summarized. As mentioned before the space group $R\bar{3}c$ is assigned to $LaAlO_3$. If hexagonal axes are chosen, the ions are in the positions: La in 6(a) $(0, 0, \frac{1}{4})$, Al in 6(b) $(0, 0, 0)$, and O in 18(e) $(x, 0, \frac{1}{4})$. Unfortunately, the oxygen parameter x cannot be derived from the X-ray diffraction patterns, because reflections indicating deviations from the ideal value of 0.5, are hardly visible. Because scattering factors are more favourable in the neutron scattering technique, a powder diffraction pattern has also been gathered. The lattice parameters from this study are also given in Table 3. For the oxygen fractional coordinate the value 0.5246 has been obtained, which agree with the value published earlier $x = 0.525$ [34]. However, in that preliminary paper less accurate cell parameters have been given.

Table 3

Hexagonal lattice constants for $LaAlO_3$ as a function of the temperature

T (K)	a (Å)	c (Å)	x (0)	ref.
113	5.356 (1)	13.089 (6)		this work
293	5.362 (1)	13.111 (5)		this work
296	5.364	13.109		[12]*)
?	5.365	13.11	0.525**)	[31]*)
300	5.364 (1)	13.105 (2)	0.5245 (5)**)	this work
473	5.369	13.129		
573	5.374	13.147		
673	5.378	13.164		
723	5.381	13.175		[12]*)
798***)	5.384	13.188		
923	5.392	13.209		
1073	5.402	13.233		
1323	5.421	13.278		

*) Accuracy not mentioned.
**) Neutron diffraction results.
***) Above this temperature cubic.

The phase transition in $LaAlO_3$ is usually described [7] by the rotation of the AlO_6 octahedra around the C_3 symmetry axes, which are parallel with the c-axis of the hexagonal cell. Although the data of Table 3 are not completely consistent due to the small deviation of the cubic symmetry, some general conclusions can be drawn. The cell parameter c changes almost linearly with the temperature except for $T < 250$ K. The phase transition is only visible in the cell parameter a, which is larger in the rhombohedral phase than expected from an extrapolation of the cubic phase. Therefore, the generally used description of a lattice compressed along the c-axis is not quite correct. Moreover, the phase transition cannot be described by a rotation of the AlO_6 octahedra alone, because in that case the cell parameter a should be smaller than expected from an extrapolation of the cubic phase. Therefore, it seems that these descriptions of the phase transition are inspired more by the actual structure of $LaAlO_3$ at low temperature, than by the change of the cell parameters at different temperatures. Nevertheless, the shift of the oxygens may be seen as a rotation of the octahedra (Fig. 6).

The structural data can be explained, if it is assumed that the La^{3+} ions tend to lower their coordination number by rotating the octahedra with decreasing temperature. Presumably to lower the strain between the AlO_6 octahedra a relative increase of the cell parameter a results.

This model offers the possibility to derive the oxygen parameter x for other temperatures. The Al–O distance and the cell parameter c are calculated from the experimental hexagonal cell parameter a, assuming the structure to be ideally cubic. In that case the calculated parameter c is larger than experimentally observed. Subsequently, the shift Δx of the oxygen ions from their ideal positions ($x = 0.5 + \Delta x$) is found by compressing the crystal along the c-axis to the experimental value, keeping the Al–O distance constant. After appropriate mathematics the following expression is obtained:

$$(\Delta x)^2 = \frac{a^2}{24} - \frac{c^2}{144}. \tag{8}$$

For the calculations of the $A(n, m)$ parameters, it is assumed that the Gd^{3+} substitute only at the La^{3+} sites in $LaAlO_3$ due to comparable ionic radii. In Table 4 the $A(n, 0)$ parameters are shown, which have been estimated with this model for the positions of the ions in the spherical unit $La_6Al_8O_{36}$, corresponding to eight AlO_6 octahedra around the Gd^{3+} ion. Extending or reducing this spherical unit does not alter the following conclusions, although the $A(n, m)$ parameters themselves are of course changed.

The temperature dependence of the different $A(n, 0)$ parameters matches very well with the observed zero field splitting parameters (Table 2). For example, the ratio $|b(2, 0)/A(2, 0)|$ is almost constant over the calculated temperature range (51 ± 3). However, it will be difficult to relate both parameters directly due to the unknown factor θ_n. Moreover, the results are very sensitive to small changes in the cell parameters. If (8) is applied to the neutron diffraction results, wrong Δx-values are obtained both for $LaAlO_3$ and the isostructural $NdAlO_3$ [35], indicating that the model is

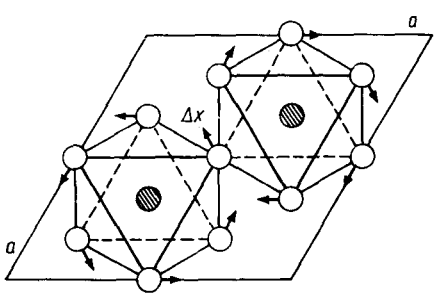

Fig. 6. Projection along the c-axis of two adjacent AlO_6 octahedra in the hexagonal cell and the shift of the oxygen ions

Table 4

Calculated crystal field parameters for $LaAlO_3$. Environment consists of $La_6Al_8O_{36}$. Δx is calculated from (8) for interpolated values of the cell parameters a and c

T (K)	a (Å)	c (Å)	Δx	$A(2, 0)$	$A(4, 0)$ (arb. units)	$A(6, 0)$
118	5.356	13.090	0.0137	−8.92	14.4	−7.17
168	5.358	13.095	0.0135	−8.66	14.4	−7.15
293	5.362	13.110	0.0126	−7.56	14.3	−7.10
413	5.367	13.127	0.0112	−5.89	14.3	−7.04
526	5.372	13.144	0.0095	−4.23	14.3	−6.98
600	5.375	13.156	0.0081	−3.05	14.3	−6.94

not exact, although in both cases the same deviation is found. However, introduction of correction factors, or changing the model, revealed the same result for the temperature dependence of the $A(n, 0)$ parameters. This indicates that the electrostatic point charge model offers at least a qualitative explanation of the observed splittings, because all models used were based on the actual cell parameters, but with different Δx.

None of these models was able to predict the distribution in $b(2, 2)$ parameters. Calculation of the $A(n, m)$ parameters yielded aside from the $A(n, 0)$ also values for $A(4, 3)$, $A(6, 3)$, and $A(6, 6)$. These values differ only slightly from those in the cubic case. Introduction of the corresponding zero field splitting parameters in the spin-Hamiltonian would cause large splittings, which have not been observed experimentally. These splittings do not correspond with the unusual broadening. Because an $A(2, 2)$ parameter has not been obtained in the crystal field calculations it is clear that the Gd^{3+} does not enter exactly the same site in $LaAlO_3$ as the La^{3+} ion. Because there is no particular $b(2, 2)$-value observed, there have to be many sites which differ only slightly from each other. It is not likely that these differences are due to differences in the degree of the rotations of the octahedra. According to (4) in that case rather a broadening of the resonances assigned to the z-direction is expected. A better explanation is obtained, if it is assumed that the Gd^{3+} ion does not fit in the $LaAlO_3$ lattice, because of its smaller ionic radius. This is supported by the fact that $GdAlO_3$ is not isostructural with $LaAlO_3$ [36]. In the structure of $GdAlO_3$ the coordination number of the Gd^{3+} ions is diminished to eight. Moreover, calculation of the $A(n, m)$ parameters by moving the Gd^{3+} ion from the centre along the principal axes shows, that $A(n, 0)$ is almost independent of this displacement, whereas among others a small $A(2, 2)$ parameter is introduced. This is in agreement with the observed zero field splitting parameters. To check this hypothesis a sample of Gd^{3+}-doped in $EuAlO_3$, which is isostructural with $GdAlO_3$, has been synthesized. Although more parameters should be introduced than given in Table 5, a first simulation of the Q-band EPR powder spectrum of this sample with only one single linewidth shows an excellent agreement

Table 5

Preliminary spin-Hamiltonian parameters for Gd^{3+} doped in polycrystalline $EuAlO_3$ at room temperature

g	$b(2, 0)$	$b(2, 2)$	$b(4, 0)$	$b(4, 2)$	$b(4, 4)$
1.983	656.4	13.8	6.7	48.6	7.2

The signs of the $b(n, m)$ (in 10^{-4} cm^{-1}) are relative to the unknown sign of $b(2, 0)$.

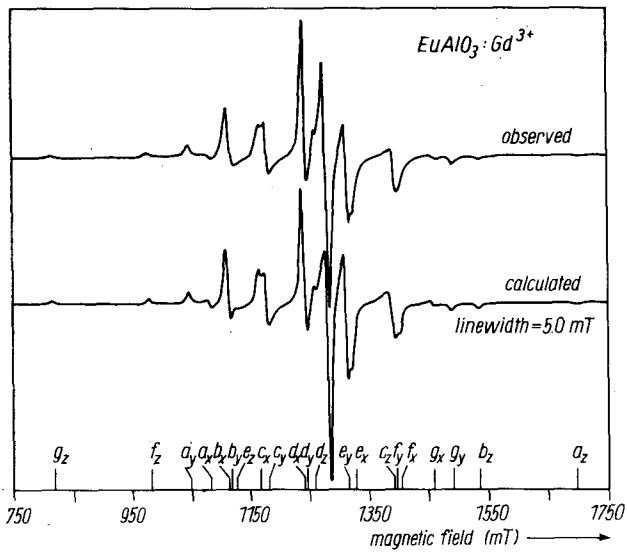

Fig. 7. Observed and calculated EPR powder spectrum of Gd^{3+}-doped $EuAlO_3$ at Q-band frequency. The calculated transitions are designated by letter according to the code in Fig. 2. Frequency 34.917 GHz, $T = 293$ K

with experiment (Fig. 7). The smaller g-value and larger linewidth than usual are due to dynamic magnetic interactions between the Eu^{3+} and Gd^{3+} ions [37].

In recent years, the superposition model of Newman [15] has frequently been used to explain the observed splittings. In this model the spin-Hamiltonian parameters $b(n, m)$ are expressed as a linear superposition of single ligand contributions

$$b(n, m) = \sum_i \bar{A}_n(R_i)\, \mathrm{K}(n, m, \theta_i, \varphi_i)\,, \tag{9}$$

where $\mathrm{K}(n, m, \theta, \varphi)$ are harmonic functions and the summation extends over the nearest-neighbour ligands situated at (R, θ, φ) of the paramagnetic ion. For the particular case considered in this paper, only the following function is required:

$$\mathrm{K}(2, 0) = \tfrac{1}{2}\,(3\cos^2\theta - 1)\,. \tag{10}$$

The intrinsic parameters $\bar{A}_n(R)$ are functions of the metal–ligand distance R and are characteristic of the ligand and paramagnetic ion in question. So far, it has been assumed that the functional form of $\bar{A}_n$ obeys a single potential law

$$\bar{A}_n(R_i) = \bar{A}_n(R_0)\left(\frac{R_0}{R_i}\right)^{t_n}, \tag{11}$$

where the exponent t_n is typical for the particular system considered. R_0 is a reference distance, usually taken as the average value of all R_i's. Substitution of (11) into (9) gives

$$\bar{A}_2(R_0) = b(2, 0)\left\{\sum_j \left(\frac{R_0}{R_j}\right)^{t_n} \mathrm{K}(2, 0)\right\}^{-1} \tag{12}$$

which means, that a single particular value for $\bar{A}_2(R_0)$ should be found if the correct value of t_n is introduced. Testing of this relation by changing t_n from -20 to $+20$ (which exceeds the usual range of this parameter), did not yield any particular value of $\bar{A}_2(R_0)$ for the model of the phase transition of $LaAlO_3$ discussed above or any other model investigated. In many cases the reverse route is followed by introducing an

$\overline{A}_2(R_0)$ value from the literature and calculating (R, θ, φ) of the ligands. However, this is of course not a proof of the correctness of this theory, because the calculated displacements cannot be determined independently. Therefore, it seems more adequate to calculate the positions of the surrounding ions first by evaluating the minimum potential energy of the Gd^{3+} ion in the host lattice. Thereafter, the zero field splitting parameters can be calculated by theory and compared with the experimental $b(n, m)$ parameters. Similar conclusions have also been reached by Bijvank et al. [38].

5. Conclusions

The simulation of the EPR powder spectrum of Gd^{3+}-doped $LaAlO_3$ shows clearly that is possible to derive spin-Hamiltonian parameters from such spectra at least in not too complicated systems as the axial cases are. It is also shown that this can only be done, if a complete simulation of both the resonance positions and the intensities is given. Otherwise, it would not have been noted that the Gd^{3+} ion does not fit in the $LaAlO_3$ lattice, which has never been reported before. In connection with this fact it might be a good suggestion to check the spin-Hamiltonian parameters obtained from single crystal measurements by calculating the simulation of the corresponding powder spectra.

Although a direct relation between observed and calculated parameters has not yet been obtained, it is clear that the electrostatic point charge model is undervalued in the literature. In the case of $LaAlO_3$ at least this model gives a qualitative explanation of the observed splittings, whereas the superposition model does not.

Acknowledgements

The authors are very grateful for the hospitality of Dr. Ir. D. C. Koningsberger and Drs. J. H. M. C. Wolput, who made it possible to perform the high-temperature measurements of the EPR spectra in their laboratory of the Eindhoven University of Technology. Thanks are also due to Mr. J. F. Strang and Dr. R. B. Helmholdt of the Energie-onderzoek Centrum Nederland at Petten for the collection of the neutron diffraction data.

References

[1] C. G. F. Stenger and A. J. Burggraaf, J. Phys. Chem. Solids **41**, 17 (1980).
[2] T. van Dijk and A. J. Burggraaf, phys. stat. sol. (a) **63**, 229 (1981).
[3] M. J. Verkerk, M. W. J. Hamminк, and A. J. Burggraaf, J. Electrochem. Soc. **130**, 70 (1983).
[4] M. A. Heilbron, B. Nieuwenhuijse, R. P. J. Vrijhoeven, and P. J. Gellings, Mater. Res. Bull. **11**, 1131 (1976).
[5] M. A. Heilbron, Ph. D. Thesis, Twente University of Technology, Enschede (The Netherlands) 1977.
[6] A. I. Leonov, L. A. Aksenova, N. S. Andrushchenko, Yu. P. Kostikov, L. P. Mudrolyubova, and B. A. Rotenberg, Izv. Akad. Nauk SSSR, Ser. neorg. Mater. **13**, 1069 (1977).
[7] K. A. Müller and Th. von Waldkirch, Local properties at phase transitions, North-Holland Publ. Co., Amsterdam 1976 (p. 187).
[8] S. Geller and V. B. Bala, Acta cryst. **9**, 1019 (1956).
[9] J. A. W. Dalziel, J. chem. Soc. 1993 (1959).
[10] B. Derighetti, J. E. Drumheller, F. Laves, K. A. Müller, and F. Waldner, Acta cryst. **18**, 557 (1965).
[11] C. de Rango, G. Tsoucaris, and C. Zelwer, Acta cryst. **20**, 590 (1966).
[12] S. Geller and P. M. Raccah, Phys. Rev. B **2**, 1167 (1970).
[13] W. Low and A. Zusman, Phys. Rev. **130**, 144 (1963).
[14] M. Rousseau, A. Bulou, C. Ridou, and A. W. Hewat, Ferroelectrics **25**, 447 (1980).

[15] D. J. NEWMAN and W. URBAN, Adv. Phys. **24**, 793 (1975).
[16] N. A. GODINA and E. K. KELER, Bull. Acad. Sci. URSS, Sér. Chim. **1**, 18 (1966).
[17] S. J. CAMPBELL, I. R. HERBERT, C. B. WARWICK, and J. M. WOODGATE, J. Phys. E **9**, 443 (1976).
[18] D. C. KONINGSBERGER, G. J. MULDER, and B. PELUPESSY, J. Phys. E **6**, 306 (1973).
[19] R. BERMAN, J. C. F. BROCK, and D. J. HUNTLEY, Cryogenics **4**, 233 (1964).
[20] T. VAN DIJK, R. B. HELMHOLDT, and A. J. BURGGRAAF, phys. stat. sol. (b) **101**, 765 (1980).
[21] H. M. RIETVELD, J. appl. Cryst. **2**, 65 (1969).
[22] G. E. BACON, Acta cryst. **A28**, 357 (1972).
[23] A. ABRAGAM and B. BLEANEY, Electron paramagnetic resonance of transition ions, Oxford University Press, London 1970.
[24] H. A. BUCKMASTER, Canad. J. Phys. **40**, 1670 (1962).
[25] G. VAN VEEN, J. magnetic Resonance **30**, 91 (1978).
[26] R. W. REYNOLDS, L. A. BOATNER, C. B. FINCH, A. CHATELAIN, and M. M. ABRAHAM, J. chem. Phys. **56**, 5607 (1972).
[27] PH. COURTY, H. AJOT, CH. MARCILLY, and B. DELMON, Powder Technol. **7**, 21 (1973).
[28] V. A. M. BRABERS, J. Crystal Growth **8**, 26 (1971).
[29] I. A. BONDAR and N. V. VINOGRADOVA, Izv. Akad. Nauk SSSR, Ser. khim. **5**, 785 (1964).
[30] J. E. WERTZ and J. R. BOLTON, Electron Spin Resonance, McGraw-Hill Publ. Co., London 1972.
[31] M. T. HUTCHINGS, Solid State Phys. **16**, 237 (1964).
[32] A. J. FREEMAN and R. E. WATSON, Phys. Rev. **127**, 2058 (1962).
[33] B. G. WYBOURNE, Phys. Rev. **148**, 317 (1966).
[34] C. DE RANGO, G. TSOUCARIS, and C. ZELWER, C.R. Acad. Sci. (France) **259**, 1537 (1964).
[35] M. MAREZIO, P. D. DERNIER, and J. P. REMEIKA, J. Solid State Chem. **4**, 11 (1972).
[36] S. QUÉZEL, J. ROSSAT-MIGNOD, and F. TCHÉOU, Solid State Commun. **42**, 103 (1982).
[37] F. MEHRAN and K. W. H. STEVENS, Physics Rep. **85**, 123 (1982).
[38] E. J. BIJVANK, H. W. DEN HARTOG, and J. ANDRIESSEN, Phys. Rev. B **16**, 1008 (1977).

(Received August 1, 1983)